Chapter 16
Application of RS and GIS for Determination of Various Criteria Causing Drying of Kanari River System

Ayushi Trivedi, Manoj Kumar Awasthi, and Malay Singh

Abstract Uncontrolled ground water extraction is the basic cause and foremost problem of ceasing effluent discharge into the water stream. To revive Kanari River in Jabalpur district using various technical approaches and determining the root causes of drying of the same is the main objective of this study. The technical advance toward the study was integration of LULC map by ERDAS imagine and ArcGIS which subsequently aimed of assessing the spatial and quantum recharge requirement for revival of river. The LULC classification was done on the grounds of satellite imagery of Landsat 5 thematic mapper (TM) from 1990, Landsat 8 enhanced thematic mapper (ETM) data from 2004, 2009, and Sentinel 2B data from 2019 that were used for visual assessment of development and land use trends within the area. The runoff was also calculated by the integration of ArcGIS and SCS-CN method which finally depicted the runoff in the area kept on increasing as rainfall kept on increasing following a linear trend which predicted that the infiltration opportunity decrease and ultimately resulting in decreased infiltration rate causing decreased baseflow resulted in drying of river.

Keywords Thematic map · LULC · SCS-CN method · Satellite imagery

16.1 Introduction

Despite of certainty ample amount of money is spent on rehabilitating our rivers across the globe, the science of restoration is still inconclusive. It is known that this is an integrated disciplinary perspective system requiring consolidated space of knowledge into a single empirical and conceptual framework (Pickett et al. 1994; Sinha et al. 2012). On that account, a systematic scientific approach is needed to resolve the upcoming challenges in river restoration which is multidisciplinary that is process based and prophetic. On a particular region, a river system may vary from upstream to downstream or from catchment to catchment. However, a better

A. Trivedi (✉) · M. K. Awasthi · M. Singh
Department of Soil and Water Engineering, Jawaharlal Nehru Krishi Vishwa Vidyalaya, Jabalpur, India

P. Kumar et al. (eds.), *Water Resources Management and Sustainability*,
Advances in Geographical and Environmental Sciences,
https://doi.org/10.1007/978-981-16-6573-8_16

knowledge in morphology and process of river is accessible at numerous scale (Sinha et al. 2013). The first and fundamental order data set of river management programs are obtained by the delineation of geomorphic conditions in a river system. Rivers go through everlasting adaptation for internal alterations, thus a river system never remains in a fixed state morphologically, for instance change in one channel due to alterations in the confluent channel, or due to external movement or changes in the basin's land cover (Brierley et al. 2006; Brierley and Fryirs 2005). Rivers go through everlasting adaptation for internal alterations, thus a river system never remains in a fixed state morphologically, for instance change in one channel due to amendments in the joining channel, or due to extraneous movement or change in the basin's land cover (Hohensinner et al. 2018). Analyzing the temporal perspective, it is observed that river adjustments reflect deferred counter to the previous advents and cumulative counter to recent advents (Brierley and Fryirs 2005). Boosting or curbing riverine activities or dynamics is somewhat related to universal channel adjustments overlapped by man-made activities. Modifications in the geomorphological characteristics or composition of river reach can undoubtedly influence or alter its capability to assist the habitat availability and ecological functions of a fluvial system (Hohensinner et al. 2018). Furthermore, riverine ecosystems, exceptionally, hinge on interruptions that create single portion of the system on typical basis. Forecasts utilizing mathematical models or tools (or any other scale models in laboratories) are generally used, yet there is still possibility to master about their efficiency or accuracy and a lot to upgrade on the model concepts. Lange et al. (2015) adopted a design which are model-based for reviving an urban river Panke situated in Berlin, Germany (Lange et al. 2015). This unfamiliar technique linked high resolution 2D hydraulic modeling including habitat modeling and using river-ecological expert ability in a continual way. Numerous approaches were proposed for habitat modeling then the habitat suitability maps were refined for the habitat and fish appropriateness for benthos was determined by involving clusters having distinct hydraulic prepossession. The advance basically model-based for intensification provided numerous antique advices on recent trends of shortcomings in the morphology of river, preferences for new form habitats creation, and quantitative learning on increment of applicable sites to be expected (Lange et al. 2015).

LULC classification performs an evident role in advancement or improvement of particular region. Precise and relevant knowledge of LULC are remarkably necessary for investigating diversified socio-ecological interests. This knowledge is critical in various operations including sustainable development, rural management, urban land planning, and agriculture. Remote sensing technology is broadly utilized for estimating LULC changes. Remote sensing data gathered using satellite images was extensively utilized for fetching LULC-related knowledge (Babykalpana et al. 2010; Saadat et al. 2011). There are numerous methods introduced basically for LULC classification with the advances and development of satellite handling and remote sensing technology (Sekertekin et al. 2017; Mishra et al. 2014).

Various observations and stream gaging data in various parts of the world and especially in India show that there is significant decrease in the non-monsoon river water flow notably in all river systems. This unusual recession of flow and drying of rivers

in post-monsoon period is recognized by small hydrologic units (watersheds and sub-catchments). The influenced areas particularly are watersheds and sub-catchments of rainfed areas, the major irrigation projects, downhill areas of degraded forest with diminishing soil cover, ground water overdraft areas, river stretches in the downstream which accommodate higher water uplift, underground mines, or deep open cast. The drying of rivers or flow depletion is broadly recognized firstly near the origin and then subsequently in the large hydrologic units. Rivers are suffering from flow degradation because of numerous possible reasons, including the water usage for agriculture and dam installation. But in most of the cases, the depleted flow is mainly due to climate change including increasing evaporation due to high temperature range and altering rainfall patterns. Diminishing runoff is elevating burden on freshwater resources all over the world and in India, because of high demand rate for water due to increasing population. Freshwater being a fundamental and core resource, the downward trends of the same are of great interest. Depleted river flow conclusively influences the world's climate. If less amount of freshwater is allowed in the oceans, they become more salty, which simultaneously effect temperature-driven ocean circulation patterns and salinity consequently playing integral role in climate regulation. The Food and Agriculture Organization (FAO) predicted that international agricultural production will elevate by 60% by the year 2050 for compensating growing population demand and dynamic consumption patterns. This signifies accelerated agriculture, which recommends that more water will be required for irrigation and other practices, more amount of fertilizer will be enforced to fields (resulting in more nutrient runoff), and burden will grow to focus on undeveloped parts of the remaining floodplains or catchment. The emerging challenges in recent era are reviving rivers to their natural state which is not attainable in most of the situations, creating balance between multiple functions of the river, scale and complexity, increasing unpredictability for future scenario, assuring the sustainability of river restoration, scientific approaches for river revival which draw the attention to the respective study.

16.2 Study Area

16.2.1 Kanari River Watershed

The present study is based on reviving of Kanari River originating from Ghutehi hill region located at Ghutehi village (Sihora Tehsil) in Jabalpur district of Madhya Pradesh (23° 33′ 36.73″ N and 80° 06′ 57.49″ E) at an elevation of about 490 m. Geographically, the origin of the river is positioned about 62 km to the northeast of Jabalpur. The location was tracked using Survey of India Toposheet no. 64A/2 (OSM No. F44C2), 64A/3 (OSM No. F44C3) and 55M/15 (OSM No. F44B15) (Fig. 16.1). The Kanari River lies under the subtropical region having an average mean sea level (MSL) of 399–401 m. Further, this river finally conjoined Suhar River (23°

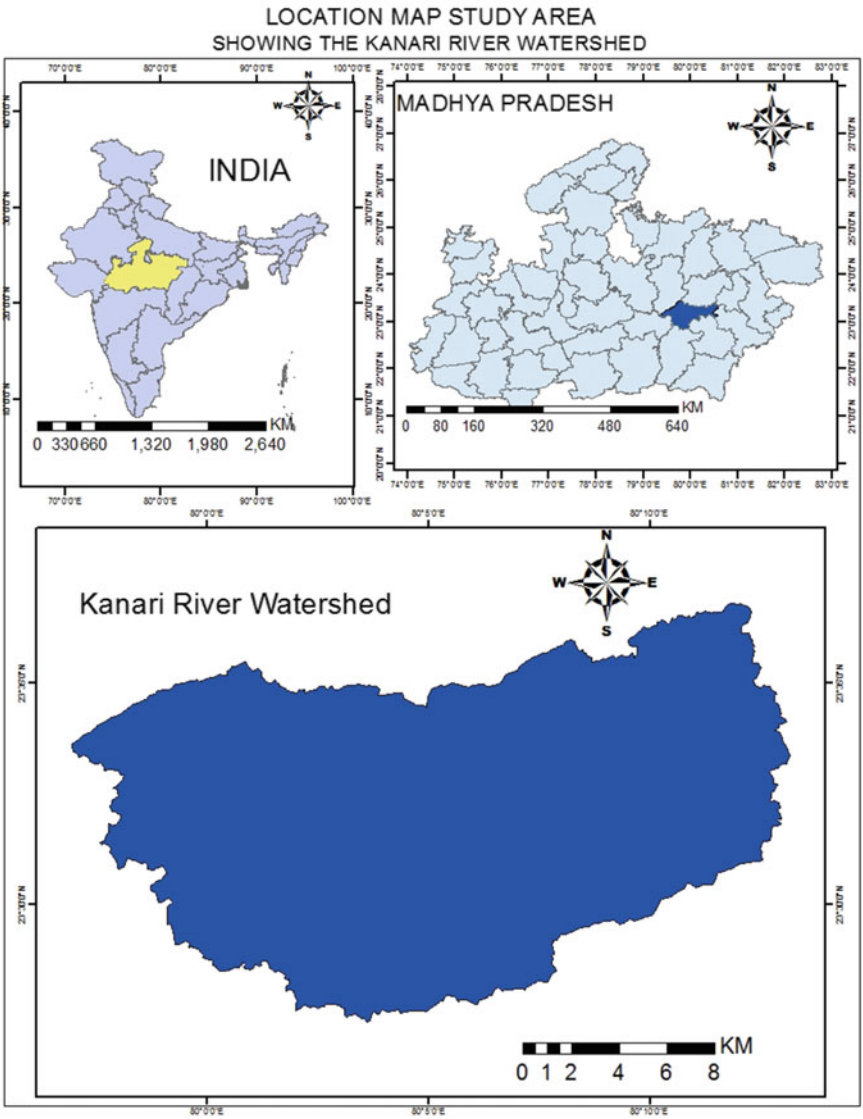

Fig. 16.1 Location map of the study area

29′ 18.68″ N and 79° 59′ 09.20″ E) in Budhi village (Majholi Tehsil) of Jabalpur (Madhya Pradesh).

The Kanari River flowing through the Sihora and Majholi Tehsil of Jabalpur is connecting about 38 g Panchayats of the area. Previously, the originating site was the hills of Gurji, Silodi, Darshani, Dinai, Khamaria, and Khudawal but gradually

due to various human interference activities and climate change scenarios, the origin of the river shifted by approximately 1.07 km.

Some of the salient features associated with the Kanari River watershed are that the river flows through the Sihora and Majhauli Tehsil of Jabalpur district. The water course of the Kanari River is 63 km long including Bah Nala which progressively conjoins the river at 23° 29′ 07.65″ N and 80° 04′ 13.45″ E. The catchment area of the river is 298 km^2. The study area involves 38 g Panchayats and 29 micro watersheds.

16.2.2 Climate

The climate of the region is mild, and generally can be classified as warm and temperate. The area receives more precipitation during the winters than in summer. The average annual temperature and precipitation of the area are about 24.6 °C and 1277 mm, respectively. The precipitation is lowest in the month of April, with an average of about 6 mm. The maximum amount of precipitation is received in the month of July and August, with an average of about 419 mm. The hottest month of the year of the area is May having an average temperature of 33.4 °C. While in the month of December and January, the average nominal temperature falls to 16.5 °C. The data collected during the period of 1982–2012 depicted that the difference in precipitation between the driest and wettest months is 413 mm/in. The maximum amount of precipitation is received in the month of July having an average of about 244.9 mm. The wind velocity is maximum in the month of June with an average of about 5 km/h.

16.2.3 Topography

The study area is surrounded by highlands having long narrow plains extending northeast and southwest. The study area is located in Jabalpur district, falling under the Mahakoshal region, situated between the watershed divide of Son and Narmada, but most of the area lies within the valley of the Narmada falling 30 ft. over a rocky ledge (the Dhuandhar, or misty shoot). The area has gentle rolling topography with an elevation difference of 1–2 m.

16.2.4 Soil

The plain of the study area which creates an offshoot from the valley of Narmada covers its southern and western portions by rich alluvial deposit including black cotton soil. The soil of the study area is black cotton soil, and water table depth is adequate near the surface.

16.3 Methodology

16.3.1 Data Products

The types of data products used in the process are as follows

For this study, satellite image of Sihora Tehsil, Jabalpur District, covering Kanari River watershed was acquired for four epochs: 1990, 2004, 2009 and 2019 from global land cover facility (GLCF) an earth science data interface (Table 16.1).

16.3.2 Software and Tools Used

Software and tools such as (a) ERDAS IMAGINE, (b) ArcGIS 10.3.1, (c) Google Earth Pro, (d) ArcInfo, (e) Microsoft Excel, and (f) Microsoft Word were used for the study. ERDAS IMAGINE was used for the image mosaic, unsupervised classification, layer stacking, AOI preparation, and accuracy assessment. ArcGIS 10.3.1 was used for watershed and subwatershed delineation, complementing the image display, various clipping features, and processing of the data. Google Earth Pro was used for validating the various features present in the study area by using sync function. ArcInfo was used for geographic input, processing, and output production. Microsoft Excel and Microsoft Word were used for graph and chart making and manuscript preparation.

16.3.3 Watershed and Subwatershed Delineation

16.3.3.1 Importing of DEM Data to ArcMap

The preliminary or foremost step was delineation of watershed and subwatershed. Previously, the delineation was carried out physically using the technique of area upstream from a certain outlet point or manually using paper maps. Currently, the same is borned out digitally in a GIS environment using ArcGIS (ESRI) desktop and Goggle Earth Pro software. For delineating Kanari River watershed, DEM data were used for determining area of interest. This DEM data were downloaded using USGS Earth Explorer.

Table 16.1 Description of various satellite images used

Image ID	Status	WRS:P/R	[UTM_ZONE]/[LATITUDE_BAND]/[GRID_SQUARE]	Acquisition date	Data set	Producer	Spatial resolution	Type
LT514404 41990008I SP00	Online	2:144/044	–	31st Nov 1990	Thematic mapper (TM)	U.S. Geological Survey (USGS)	30 * 30 m	GeoTIFF
LT514404 42004335B KT00	Online	2:144/044	–	31st Nov 2004	Thematic mapper (TM)	U.S. Geological Survey (USGS)	30 * 30 m	GeoTIFF
LT514404 42009332 KHC00	Online	2:144/044	–	31st Nov 2009	Thematic mapper (TM)	U.S. Geological Survey (USGS)	30 * 30 m	GeoTIFF
S2B_MSIL 1C_201903 20T050649 _N0207_R 019_T44Q MM_2019 0320T1026 53	Online	–	Military grid reference system/52.3140232/2B	31st Nov 2019	Multispectral sensor (MSS)	U.S. Geological Survey (USGS)	10 * 10 m	GeoTIFF

16.3.3.2 Delineation of Kanari River Watershed

The DEM grid was set as input surface raster for processing. Fill tool from the Hydrology toolbox (ArcGIS 10.3.1) was utilized for removing any sort of imperfections or (sinks) in the digital elevation model (DEM). The output surface raster was also added to the working directory. The flow direction tool was used for creating flow direction grids. The grid processor was used for finding the lowest neighboring cell from the center (for every 3 * 3 cell neighborhood). The working directory was also updated with output surface raster. Each of the specified number in the listed matrix below depicts the flow direction—that is, on the assumption that the center cell flows northeast, its value will be assumed 128; if they flows due north, its value will be 64, etc. For calculating the flow in each call, the flow accumulation tool was used and simultaneously the upstream cells was identified that flow in each downslope cell (Fig. 16.2). Nevertheless, each cell's flow accumulation value was estimated by the number of cells flowing upstream based on topography and landscape. The flow accumulation layer was now symbolized for enhancing the visual quality of pinpoint areas having high flow accumulation. Outlet (pour) points were created by providing the latitude and longitude value in ArcCatalog window by using start and stop editing dialog box (viz. 23° 29′ 18.68″ N and 79° 59′ 09.20″ E). The tool, namely snap pour point, was applied for accomplishment of two things, that is, snaping of the pour point created to the nearest cell of high flow accumulation for accounting any error at the time of placement and to convert the pour points into the raster format for watershed tool input. Eventually, the watershed was delineated using Hydrology tool in ArcCatalog window.

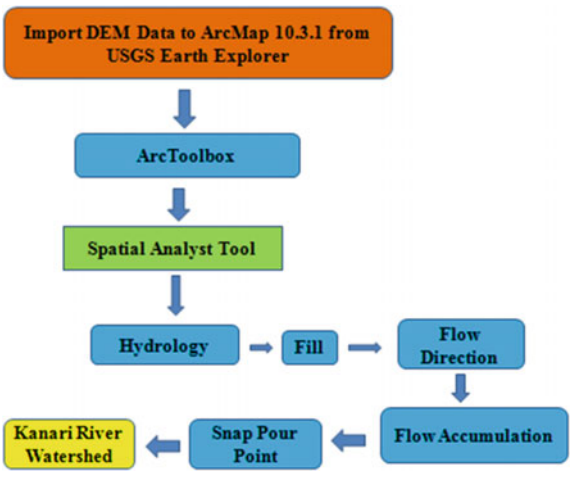

Fig. 16.2 Delineation of Kanari River watershed

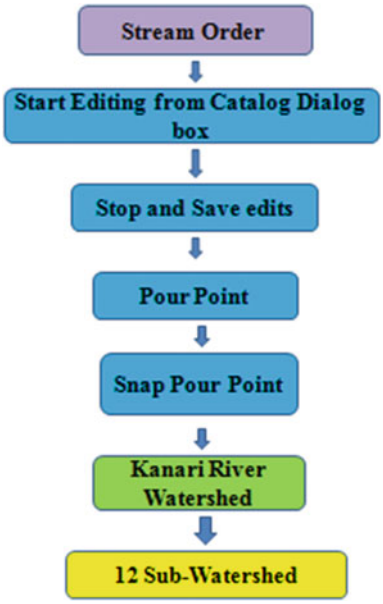

Fig. 16.3 Delineation of Kanari River subwatershed

16.3.3.3 Delineation of Kanari River Subwatershed

Stream link function was used for creating a grid of stream segments (or links) having unique identification (Fig. 16.3). This provide the clarification that whether a link is a head link, or it is a conjunction between two links. In a particular link, all the cell must have the similar grid code that is specified to that link. The DEM used for deriving raster representation was simultaneously converted in vector format representation. Strahler stream order function from hydrology tool was eventually used to calculate the number of stream order present in the catchment area. It is of great importance to delineate or determine watersheds draining to a specific points on the stream network, for example, stream gages. Using spatial analyst tools of ArcGIS 10.3.1 followed by Hydrology and snap pour point, the subwatersheds were delineated.

16.3.3.4 LULC Preparation

Identification, determination, and detection of digital change are the activity that assists in discovering the changes linked with the land use land cover properties with instance to multi-temporal geo-registered RS data. Identification of temporal changes (normal variation) that is generally not possible with other technologies are quite feasible. LULC change detection has many utilizations such as land use changes, rate of coastal change, afforestation/deforestation, urban sprawl, and other progressive changes through temporal and spatial analysis tools and techniques such as RS and geographic information system (GIS) in conjunction with digital image

processing techniques. For supporting LULC, land use change models (LUCM) mostly treated as an efficient tool for analyzing the root causes of land use land cover change and related consequences. In addition, the LULC model is also effective in anticipating the post or future scenario and analyzing spatial, temporal distribution of LULC utilizing the gained observation from last or previous years (Islam et al. 2018). Number of researchers and scientists, such as Singh et al. (2001a, b, c, d, e), Dey and Singh (2003), Okada et al. (2001), and Dey et al. (2004), conducted researches associated with ocean, surface, and atmospheric variables or parameters.

For preparing LULC map using satellite images, types of classification scheme which basically define or prescribe the LULC classes were taken into consideration. The different number of LULC classes were decided on the basis of requirement of a definite program for peculiar implication or operation (Arora and Mathur 2001; Saha et al. 2005). Eight primary LULC classes were selected for mapping the unified watershed area viz.; waterbody, agricultural land, forest/mountain, wasteland, open land, mines, habitat, and vegetation. Area under dry, irrigated or rainfed agricultural land was enclosed as agricultural land mean while space occupied by agroforestry was considered as forest class because of analogous spectral and spatial response of the tree cover in agroforestry systems to open forests. After preparing classification system, most extensively used image classification system or approach, i.e., maximum likelihood classification was used for mapping all types of land use/cover classes (Fig. 16.4). Before selecting the training samples, satellite imagery was analyzed empirically; Toposheet of the watershed and Google Earth images were also investigated carefully and simultaneously unsupervised classification then into 50 classes. There were many places where land use/land cover was different from actual land use/land cover. So, in order to correct it and for improving the accuracy assessment, AOI was drawn for each and every wrong land use/land cover.

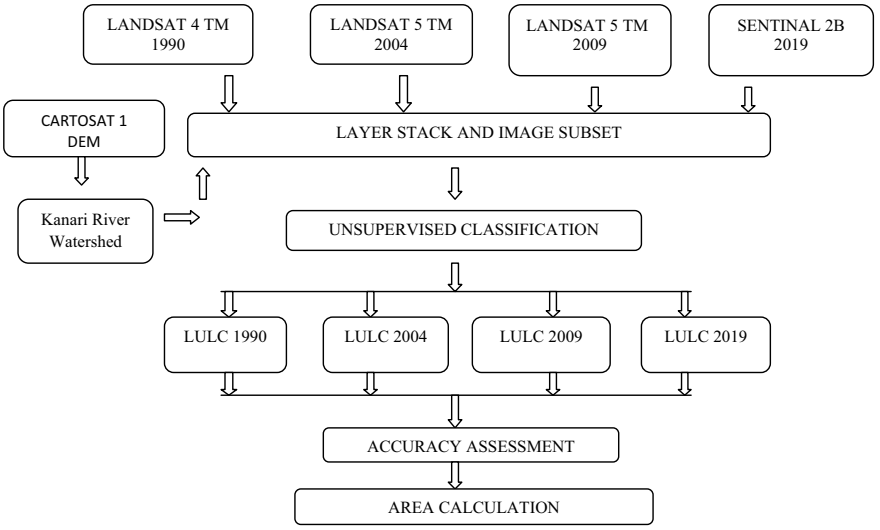

Fig. 16.4 Flowchart for LULC preparation

16.4 Results and Discussion

16.4.1 Delineation of Kanari River Watershed and Subwatershed

Firstly, the SRTM DEM was processed using ArcGIS. The basin of Kanari River was delineated utilizing the Hydrology tool of ArcGIS (ESRI), ArcHydro tools. Numerous automatic watershed delineation techniques and tools generated different areal extents of the basin and stream networks using DEMs. These steps viz., fill, flow direction, flow accumulation, watershed outlet (pour point), stream order, watershed, pour point, and subwatershed are depicted in Fig. 16.5.

The drainage pattern observed in the Kanari basin is homogeneous in nature and having the drainage density of 0.93 km^{-1}. Stream ordering was accomplished using drainage network and DEM in ArcGIS using Hydrology tool as depicted in Fig. 16.6. Drainage network is utilized for watershed delineation and for proposing numerous soil conservation measures and water harvesting structures.

16.4.2 LULC Preparation

Multi-temporal and multi-spectral LULC map consisting of eight major (main) classes: waterbody, agricultural land, forest/mountain, wasteland, open land, mines, habitat, and vegetation of 1990, 2004, 2009 and 2019 are depicted in Figs. 16.7 and 16.8. Obtained spatial and spectral distribution pattern of LULC using unsupervised classification are depicted in Table 16.2.

Area wise comparison of different years on the basis of LULC map prepared is illustrated in Fig. 16.9 showing devastated decrease in water bodies and forest land.

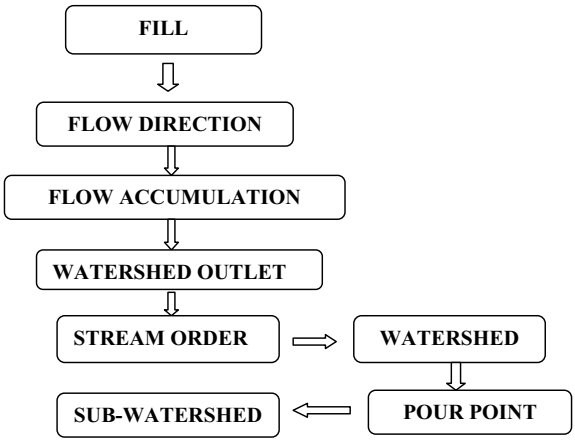

Fig. 16.5 Delineation of Kanari River watershed

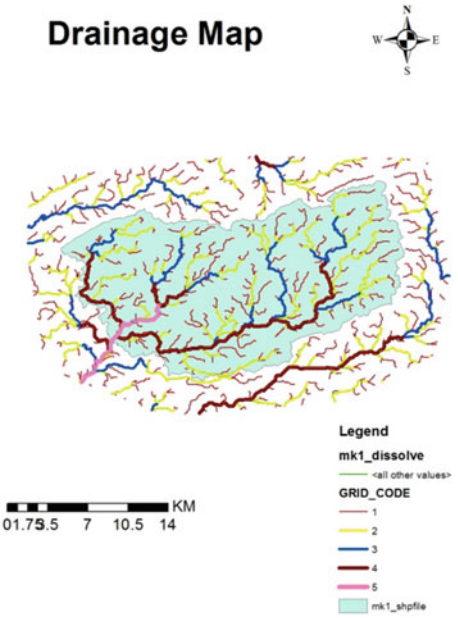

Fig. 16.6 Drainage map of Kanari River watershed

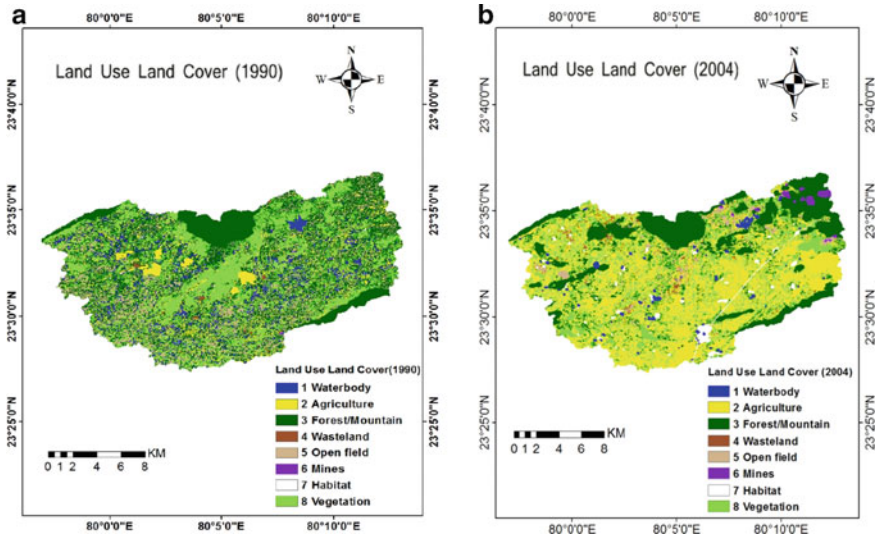

Fig. 16.7 LULC map for the year 1990 and 2004

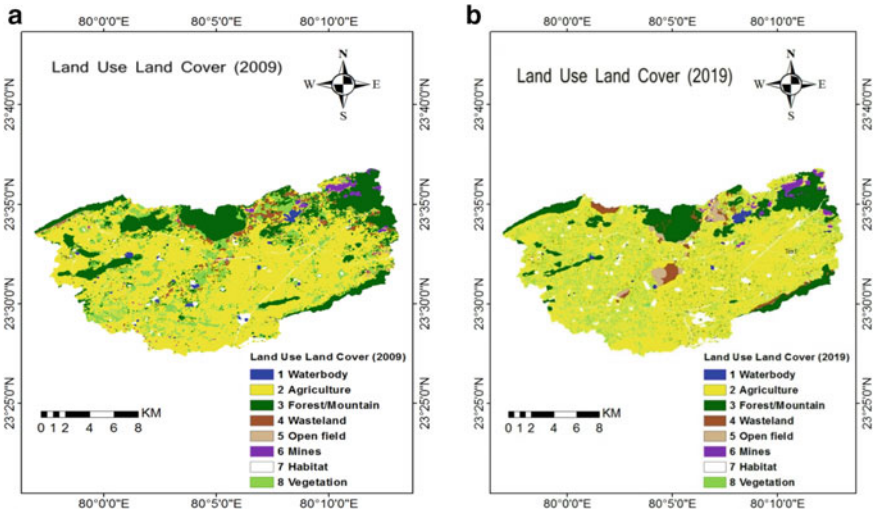

Fig. 16.8 LULC map for the year 2009 and 2019

The graphical comparison of all the eight classes on the basis of areal distribution obtained from LULC map was also analyzed and is shown in Fig. 16.10 illustrating rising and falling linear trend of different parameters. The classified maps depicted that in the year 1990 area under different classes viz.; agricultural land was 9.80%, wasteland was 0.40%, mining activity was 0.154%, habitat area covered 0.493%, dense forest and vegetation covering major portion of the watershed, and covered about 40.06% and 28.52% space, respectively. While in the year 2004, about 43.09% of the space was covered by agricultural land against 9.80% space in 1990 clearly noticed an increment in cultivated land area. Waste land, mines, and habitat area covered 1.16%, 0.879%, and 2.57%, respectively while agriculture had greatest share of 43.09% over open forest 25.65%. The water body share was about 1.339% of the total geographical area for the year 2004 (Table 16.2; Fig. 16.11).

The classified image for the year 2009 depicted that above 50% of the space was occupied by agricultural land, whereas open forest share was 21.84%. Vegetation occupied 10.34%; habitat area covered 2.68% while waste land and water bodies occupied 2.88% and 0.89% (less than 1%) area, respectively. In 2019, the area under agricultural field has fairly grown and covered 61.86% collectively whereas forest lands depleted to 14.76%. Mines and habitat covered 1.205% and 5.40% area, respectively, resulting in depletion of waterbody to minimal amount that is only 0.625% (< 1%) (Table 16.2).

Table 16.2 LULC distribution in Kanari river watershed of Jabalpur

LULC classes	1990		2004		2009		2019	
	Area (ha)	Area (%)	Area (ha)	Area (%)	Area (ha)	Area (%)	Area (ha)	**Area (%)**
Waterbody	2366.45	7.910807	400.68	1.339433	268.38	0.897168	187.11	0.62549
Agriculture	2933.7	9.807068	12,891.8	43.09601	16,981.5	56.76747	18,507.1	61.8674
Forest/mountain	11,984.7	40.06366	7675.83	25.65954	6535.08	21.84612	4417.92	14.76867
Wasteland	119.827	0.40057	347.58	1.161925	862.11	2.881948	1205.64	4.030335
Openfield	3771.41	12.60745	1212.84	4.054404	1052.01	3.516765	591.75	1.978161
Mines	46.1703	0.154343	263.16	0.879718	316.44	1.057828	360.63	1.20555
Habitat	147.763	0.493957	770.67	2.576273	803.79	2.68699	1617.8	5.408145
Vegetation	8533.41	28.52634	6377.58	21.31962	3094.83	10.34571	3030.39	10.13029
Total	29,914.14		29,914.14		29,914.14		29,914.14	

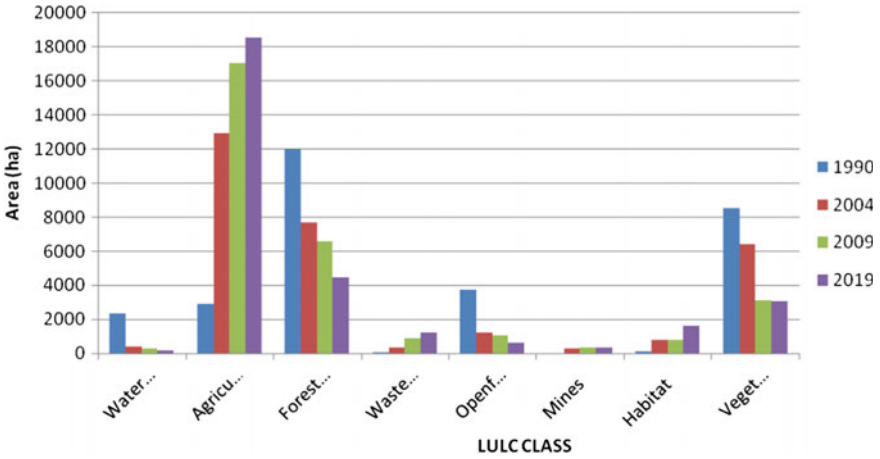

Fig. 16.9 LULC area wise comparison of different years

16.4.3 Field Survey and Accuracy Assessment

The ground truthing was performed at different levels involving personal interview with the resident of the area for validating the path of the river and determination of causes of flow cessation. Some of the photograph of the field survey and ground truthing are illustrated in Fig. 16.12.

Kappa accuracy assessment which is one of the most generously used approaches was selected for assessing the accuracy of classified map of the year 1990, 2004, 2009, and 2019. Accuracy assessment was also performed using satellite imagery having high resolution of Planet scope 100 stratified random points with minimum 12 points in each class were generated. User's accuracy and individual producer's accuracy of all the classes are also presented**.**

Accuracy assessment for the year 1990

The overall classification accuracy for the obtained classified image of 1990 was determined and was 63% having overall Kappa coefficient of 0.5734 (Tables 16.3 and 16.4).

Accuracy assessment for the year 2004

The overall classification accuracy for the obtained classified image of 2004 was determined and was 83% having overall Kappa coefficient of 0.8016 (Tables 16.5 and 16.6).

Accuracy assessment for the year 2009

The overall classification accuracy for the obtained classified image of 2009 was determined and was 90% having overall Kappa coefficient of 0.8690 (Tables 16.7 and 16.8).

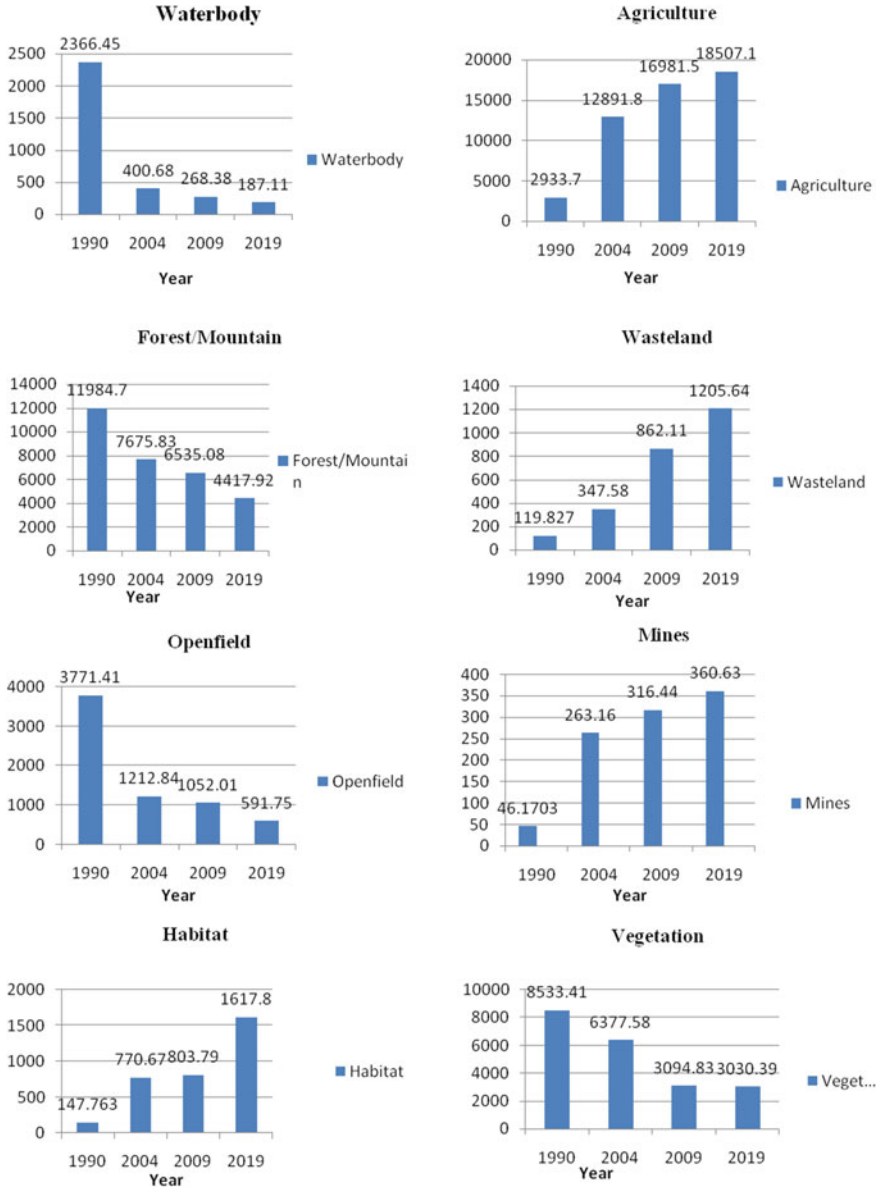

Fig. 16.10 LULC area wise comparison of different years of eight classes

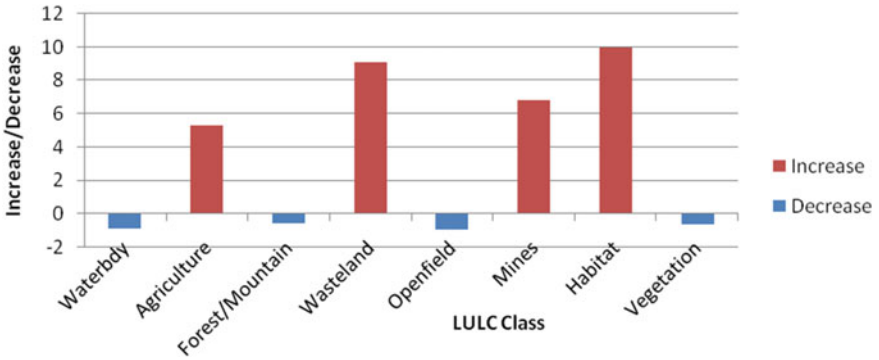

Fig. 16.11 Increase/decrease in area (ha) of eight classes

Fig. 16.12 Photograph captured during ground truthing and accuracy assessment

Table 16.3 Classification accuracy

LULC class	Reference total	Classified total	Number correct	Producers accuracy (%)	Users accuracy (%)
Waterbody	9	12	7	77.78	58.33
Agriculture	16	12	7	43.75	58.33
Forest/mountain	17	18	8	47.06	44.44
Wasteland	6	10	6	100.00	60.00
Openfield	13	12	7	53.85	58.33
Mines	9	10	8	88.89	80.00
Habitat	11	10	8	72.73	80.00
Vegetation	19	16	12	63.16	75.00

Table 16.4 Overall Kappa statistics

LULC class	Kappa
Waterbody	0.5421
Agriculture	0.504
Forest/mountain	0.3307
Wasteland	0.5745
Openfield	0.5211
Mines	0.7802
Habitat	0.7753
Vegetation	0.6914

Table 16.5 Classification accuracy

LULC class	Reference total	Classified total	Number correct	Producers accuracy (%)	Users accuracy (%)
Waterbody	9	10	9	100.00	90.00
Agriculture	26	23	18	69.23	78.26
Forest/mountain	13	13	13	100.00	100.00
Wasteland	9	11	8	88.89	72.73
Openfield	7	10	6	85.71	60.00
Mines	8	10	8	100.00	80.00
Habitat	12	11	11	91.67	100.00
Vegetation	16	12	10	62.50	83.33

Accuracy assessment for the year 2019

The overall classification accuracy for the obtained classified image of 2019 was determined and was 87.34% having overall Kappa coefficient of 0.8390 (Tables 16.9 and 16.10).

Table 16.6 Overall Kappa statistics

LULC class	Kappa
Waterbody	0.8901
Agriculture	0.7062
Forest/mountain	1
Wasteland	0.7003
Openfield	0.5699
Mines	0.7826
Habitat	1
Vegetation	0.8016

Table 16.7 Classification accuracy

LULC class	Reference total	Classified total	Number correct	Producers accuracy (%)	Users accuracy (%)
Waterbody	3	5	3	100.00	60.00
Agriculture	42	42	38	90.48	90.48
Forest/mountain	17	18	17	100.00	94.44
Wasteland	7	6	6	85.71	100.00
Openfield	8	9	7	87.50	77.78
Mines	5	5	5	100.00	100.00
Habitat	7	6	5	71.43	83.33
Vegetation	11	9	9	81.82	100.00

Table 16.8 Overall Kappa statistics

LULC class	Kappa
Waterbody	0.5876
Agriculture	0.8358
Forest/mountain	0.9331
Wasteland	1
Openfield	0.7585
Mines	1
Habitat	0.8208
Vegetation	1

Runoff estimation using integration of SCS-CN method and ArcGIS

The methodology applied for runoff calculation is depicted in Fig. 16.13. The soil conservation service curve number approach is usually utilized empirical methods to determine the direct runoff from a drainage basin (USDA 1972) in the Kanari basin. The surface storage is combined with infiltration losses by the relation of

Table 16.9 Classification accuracy

LULC class	Reference total	Classified total	Number correct	Producers accuracy (%)	Users accuracy (%)
Waterbody	6	10	4	79.67	79.00
Agriculture	59	23	19	82.20	82.61
Forest/mountain	4	13	2	87.98	96.87
Wasteland	3	11	2	86.67	18.18
Openfield	4	10	1	87.00	69.00
Mines	3	10	3	100.00	87.00
Habitat	6	11	2	79.87	91.87
Vegetation	19	12	7	83.84	58.33

Table 16.10 Overall Kappa statistics

LULC class	Kappa
Waterbody	0.7617
Agriculture	0.7758
Forest/mountain	1
Wasteland	0.8754
Openfield	1
Mines	0.7976
Habitat	0.8976
Vegetation	0.9321

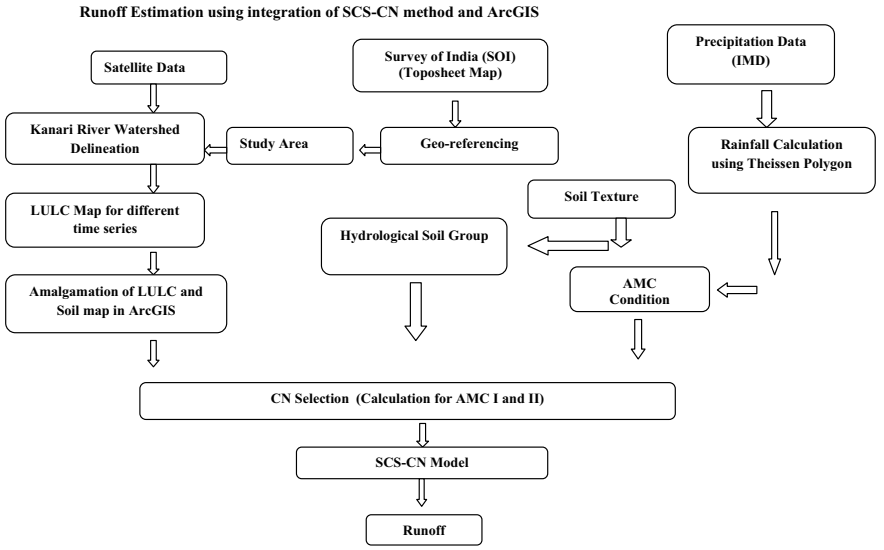

Fig. 16.13 Methodology for runoff calculation

$$Q = (P - \text{Ia})^2 / P - \text{Ia} + S \tag{16.1}$$

Here,

Q gathered/collected runoff (mm),
P effective rainfall depth (mm),
Ia initial abstraction (mm) (surface storage, interception, and infiltration preceding to runoff in the entire watershed). The empirical relation was obtained in the terms of Ia and is depicted below.

The empirical relationship is

$$\text{Ia} = 0.3S \tag{16.2}$$

The potential maximum retention (S) for Indian conditions is given by

$$S = \left(\frac{25{,}400}{\text{CN}}\right) - 254 \tag{16.3}$$

where

CN curve number (source: USDA 1972).

Rewriting the equation as

$$Q = (P - 0.3S)^2 / (P + 0.7S) \tag{16.4}$$

The runoff from the entire area was calculated in significance of value of CN using Eqs. 16.3 and 16.4.

The SCS curve number serves the determination of capability of soils to accommodate infiltrated water in regards of land use/ land cover (LULC) and antecedent soil moisture condition (AMC) (Amutha and Porchelvan 2009) (Table 16.11). U.S soil conservation service (SCS) soils distributed the soil into four hydrologic soil groups, namely group A, B, C, and D, in regards of probable rate of runoff and final infiltration. CN, S, and P calculated for various years are shown in Table 16.12.

Table 16.11 Antecedent soil moisture classes (AMC) group

AMC group	Soil characteristics	Five-day antecedent rainfall in mm	
		Dormant season	Growing season
I	Wet condition	< 13	< 36
II	Average condition	13–28	36–53
III	Heavy condition	> 28	> 53

Table 16.12 Hydrological and quantitative calculations in the watershed

AMC	CN				*S*				$P > 0.3S$			
	1990	2004	2009	2019	1990	2004	2009	2019	1990	2004	2009	2019
I	67.75	71.33	73.48	75.06	120.88	102.06	91.64	84.38	36.26	30.61	27.49	25.3
II	82.76	85.05	86.37	87.32	52.91	44.63	40.06	36.88	15.86	13.38	12.01	11.0
III	92.00	93.02	93.68	94.16	22.07	19.05	17.10	15.74	6.62	5.71	5.13	4.24

Table 16.13 Aimed weighted curve number (WCN) at Kanari River watershed for the year 1990

Land use cover	Soil type (HSG)	Area in ha	Area in m^2	CN	Area	Area * CN	Weighted curve number (WCN)
Waterbody	D	2265.4	22,654,000	100	0.075757	7.575728	AMC I—67.75 AMC II—82.76 AMC III—92.00
Agriculture	D	2941.15	29,411,500	90	0.098355	8.851954	
Forest/mountain	D	12,028.5	120,285,000	77	0.402245	30.97289	
Wasteland	D	119.827	1,198,270	94	0.004007	0.376671	
Openfield	D	3780.12	37,801,200	84	0.126411	10.61853	
Mines	D	46.7092	467,092	95	0.001562	0.14839	
Habitat	D	149.38	1,493,800	86	0.004995	0.429606	
Vegetation	D	8572.31	85,723,100	83	0.286667	23.79334	
Total			299,033,962			82.76711	

It was found from the calculations (SCS method), annual surface runoff depth (465.59 mm) for the year 1990 are multiplied by watershed area (A = 299,033,962 m^2) provides the total average runoff volume as (139,228,136.1 m^3). The result for the year 1990 is depicted in Table 16.13.

It was found from result of the calculations (SCS method), annual surface runoff depth (597.21 mm) for the year 2004 is multiplied by watershed area (A = 299,033,962 m^2) provides the total average runoff volume as (178,807,886.9 m^3). The result for the year 2004 is depicted in Table 16.14.

It was found from the calculations (SCS method), annual surface runoff depth (737.44 mm) for the year 2009 are multiplied by watershed area (A = 299,033,962 m^2) provides the total average runoff volume as (220,599,996.4 m^3). The result for the year 2009 is depicted in Table 16.15.

It was found from the calculations (SCS method), annual surface runoff depth (1319.24 mm) for the year 2019 are multiplied by watershed area (A = 299,033,962 m^2) provides the total average runoff volume as (361,883,866 m^3). The result for the year 2019 is depicted in Table 16.16.

The runoff varies 465.59–1319.24 mm (1990–2019) as shown in Table 16.17. The amount of rainfall varies between 1136.7 and 2466.9 mm in the Kanari River watershed as shown in Table 16.17. The calculated average annual runoff is found to

Table 16.14 Aimed weighted curve number (WCN) at Kanari River watershed for the year 2004

Land use cover	Soil type (HSG)	Area in ha	Area in m^2	CN	Area	Area * CN	Weighted curve number (WCN)
Waterbody	D	400.68	4,006,800	100	0.013383	1.33827	AMC I—71.33 AMC II—85.05 AMC III—93.02
Agriculture	D	12,891.8	128,918,000	90	0.430586	38.75272	
Forest/mountain	D	7675.83	76,758,300	77	0.256373	19.74069	
Wasteland	D	347.58	3,475,800	94	0.011609	1.091261	
Openfield	D	1212.84	12,128,400	84	0.040509	3.402742	
Mines	D	263.16	2,631,600	95	0.00879	0.835006	
Habitat	D	770.67	7,706,700	86	0.02574	2.213671	
Vegetation	D	6377.58	63,775,800	83	0.213011	17.67992	
Total			299,033,962			85.05428	

Table 16.15 Aimed weighted curve number (WCN) at Kanari River watershed for the year 2009

Land use cover	Soil type (HSG)	Area in ha	Area in m^2	CN	Area	Area * CN	Weighted curve number (WCN)
Waterbody	D	268.38	2,683,800	100	0.008972	0.897168	AMC I—73.48 AMC II—86.37 AMC III—93.68
Agriculture	D	16,981.5	169,815,000	90	0.567675	51.09072	
Forest/mountain	D	6535.08	65,350,800	77	0.218461	16.82152	
Wasteland	D	862.11	8,621,100	94	0.028819	2.709031	
Openfield	D	1052.01	10,520,100	84	0.035168	2.954083	
Mines	D	316.44	3,164,400	95	0.010578	1.004936	
Habitat	D	803.79	8,037,900	86	0.02687	2.310812	
Vegetation	D	3094.83	30,948,300	83	0.103457	8.586939	
Total			299,033,962			86.3752	

be 779.87 mm and average runoff volume for the period of 29 years is 225,129,971.3 m^3. The rainfall runoff relationship showed in Fig. 16.14 for Kanari watershed. Rainfall-runoff variation in Kanari watershed is showed in Figs. 16.15 and 16.16, respectively depicting rising linear trend in aspect of both the parameters simultaneously decreasing opportunity time and hence infiltration decreasing baseflow of the area.

Table 16.16 Aimed weighted curve number (WCN) at Kanari River watershed for the year 2019

Land use cover	Soil type (HSG)	Area in ha	Area in m^2	CN	Area	Area * CN	Weighted curve number (WCN)
Waterbody	D	187.11	1,871,100	100	0.006254	0.625402	AMC I—75.06 AMC II—87.32 AMC III—94.16
Agriculture	D	18,507.1	185,071,000	90	0.618587	55.67284	
Forest/mountain	D	4417.92	44,179,200	77	0.147666	11.37028	
Wasteland	D	1205.64	12,056,400	94	0.040298	3.787983	
Openfield	D	591.75	5,917,500	84	0.019779	1.661422	
Mines	D	360.63	3,606,300	95	0.012054	1.145112	
Habitat	D	1617.8	16,178,000	86	0.054074	4.650352	
Vegetation	D	3030.39	30,303,900	83	0.101289	8.406963	
Total			299,033,962			87.32035	

Table 16.17 Annual average runoff depth and volume

Year	Rainfall in mm	Runoff in mm	Volume (m^3) = (Runoff * area)	Runoff Co. = (RO/RF)
1990	1136.7	465.59	139,228,136.1	0.4
2004	1220.38	597.22	178,807,886.9	0.48
2009	1225.1	737.44	220,599,996.4	0.6
2019	2466.9	1319.25	361,883,866	0.49
Average	1512.27	779.8750954	225,129,971.3	0.49

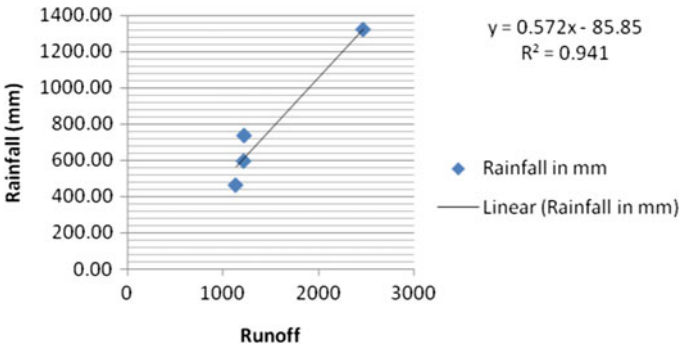

Fig. 16.14 Scatter plot between the rainfall and calculated runoff

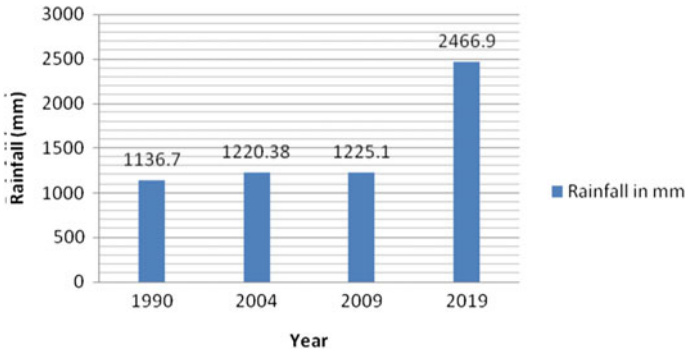

Fig. 16.15 Rainfall variation in Kanari watershed

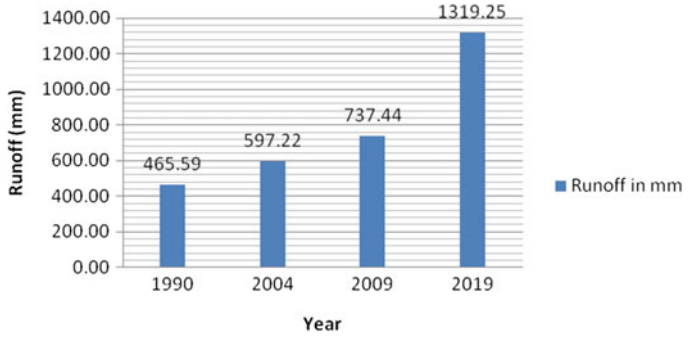

Fig. 16.16 Runoff variation in Kanari watershed

16.5 Conclusion

Remote sensing (RS) and geographic information system (GIS) technology is one of the broadly or extensively applied science used for detection analysis of land use and land cover change. The detection of land use change criterion for Kanari River watershed was performed using downloaded satellite images and was further classified utilizing ERDAS imagine 2014 software. The observations of the study finally concluded that there were significant change in land use land cover over the period of 29 years in Kanari River watershed. There was significant rise in agriculture land by about 53.08% and a downfall in water bodies by about 92.07% from the year 1990–2019. The classification scheme utilized eight LULC classes representing urban/built-up areas (habitation), vegetation, forest, wasteland, open field, water features, agriculture field, and mined area for the year 1990, 2004, 2009 and 2019. The classification method used for this project produced an overall accuracy of 93.4% which finally interpreted contrasting percentage of various classes that resulted in drying of the river. The result indicated that the habitation and mining

activities was increased by 98.3% and 67.2% (form the year 1990 to 2019), respectively, which consequently enhanced the groundwater overdraft. Further analysis showed that the forest (63.2% decrease), vegetation (64.64% decrease), and water body (91.7% decrease) acreage were converted into waste land (90.61% increase), agriculture field (52.92% increase) resulted in shifting of the origin of the river by 1.07 km obtained during ground truthing. The forest area was chiefly converted into habitat land as a result of incremented population leading to high requirement rate in the area. This was associated to the continued extension of settlement and cultivated over period of years in Kanari River watershed. The science about the land use change is pre-requisite for land use planning and administration activities in Kanari River watershed. Therefore, this study revealed that there was an increase of mined area and habitat which was the root cause of drying of the river. Curve number and soil conservation service model were utilized in the study by analyzing soil map and land use map described in ArcGIS, as an input data. In the current study, the methodology applied for the tenacity or determination of runoff utilizing combined SCS and GIS approach can also be applied in any other watershed for the conservation measures. The fruitful soil and water conservation measures need be designed and enforced in the watersheds for grasping or gathering runoff volume and soil loss. Antecedent moisture condition of the soil imitates a significant role in SCN curve number method accounted for estimating runoff depth.The runoff in the study area was also calculated by the integration of ArcGIS and SCS-CN method which finally depicted the runoff in the area kept on increasing as rainfall kept on increasing following a linear trend which predicted that the infiltration opportunity decrease and ultimately resulting in decreased infiltration rate causing decreased baseflow resulted in drying of river. Concluding, soil conversations service –curve number technique is handily proven as a superior method, consuming little time and facilitating handling of big data set as well as identification of suitable site for artificial recharge structures. Various questioner surveys were also conducted which indicated that direct uplifting of water from the stream for irrigation purpose is root cause of the problem.

References

Amutha R, Porchelvan P (2009) Estimation of surface runoff in Malattar sub-watershed using SCS-CN method. J Soc Remote Sens 37(2):291–304

Arora KM, Mathur S (2001) Multi-source classification using artificial neural network in a rugged terrain. Geocarto Int 16(3):37–44

Babykalpana Y, ThanushKodi K (2010) Supervised/unsupervised classification of LULC using remotely sensed data for Coimbatore city, India. Int J Comput Appl 2(7):26–30

Brierley GJ, Fryirs KA (2005) Geomorphology and river management: applications of the river styles framework. Blackwell, Oxford, pp 398

Dey S, Singh RP (2003) Surface latent heat flux as an earthquake precursor. Nat Hazards Earth Syst Sci 3:749–755

Dey S, Sarkar S, Singh RP (2004) Anomalous changes in column water vapor after Gujarat earthquake. Adv Space Res 33:274–278

Dimyati MUH, Mizuno K, Kobayashi S, Kitamura T (1996) An analysis of landuse/cover change in Indonesia. Int J Remote Sens 17(5):931–944
USDA Soil Conservation Service (1972) National engineering handbook. Hydrology section 4. Chapters 4–10. USDA, Washington, D.C.
Herold M, Gardner ME, Robert DA (2003) Spectral resolution requirements for mapping urban areas. IEEE Trans Geosci Remote Sens 41:1907–1919
Hohensinner S, Hauer C, Muhar S (2018) River morphology, channelization, and habitat restoration. In: Riverine ecosystem management. Springer, pp 41–65
Islam K, Rahman MF, Jashimuddin M (2018) Modeling land use change using cellular automata and artificial neural network: the case of Chunati wildlife sanctuary, Bangladesh. Ecol Indic 88:439–453
Kiruki HM, van der Zanden EH, Malek Z, Verburg PH (2017) Land cover change and woodland degradation in a charcoal producing semi-arid area in Kenya. Land Degr Dev 28:472–481
Lange C, Schneider M, Mutz M, Haustein M, Halle M, Seidel M, Sieker H, Wolter C, Hinkelmann R (2015) Model-based design for restoration of a small urban river. J Hydro-Environ Res 9:226–236
Mishra VN, Kumar P, Gupta DK, Prasad R (2014) Classification of various land features using risat-1 dual polarimetric data. Int Arch Photogramm Remote Sensing Spatial Inf Sci:833–837
Muhar S, Januschke K, Kail J (2016) Evaluating good-practice cases for river restoration across Europe: context, methodological framework, selected results and recommendations. Hydrobiologia 769:3–19
Niquisse S, Cabral P, Rodrigues Â, Augusto G (2017) Ecosystem services and biodiversity trends in Mozambique as a consequence of land cover change. Int J Biodivers Sci Ecosyst Serv Manage 13:297–311
Okada Y, Mukai S, Singh RP (2004) Changes in atmospheric aerosol parameters after Gujarat earthquake of January 26 2001. Adv Space Res 33:254–258
Pauleit S, Ennos R, Golding Y (2005) Modeling the environmental impacts of urban land use and land cover change—a study in Merseyside, UK. Landsc Urban Plan 71:295–310
Petit C, Scudder T, Lambin E (2001) Quantifying processes of land-cover change by remote sensing: resettlement and rapid land-cover changes in south-eastern Zambia. Int J Remote Sens 22(17):3435–3456
Read JM, Lam NSN (2002) Spatial methods for characterising land cover and detecting land-cover changes for the tropics. Int J Remote Sens 23(12):2457–2474
Saadat H, Adamowski J, Bonnell R, Sharifi F, Namdar M, Ale-Ebrahim S (2011) Land use and land cover classification over a large area in Iran based on single date analysis of satellite imagery. ISPRS J Photogramm Remote Sens 66:608–619
Saha AK, Arora MK, Csaplovics E, Gupta RP (2005) Land cover classification using IRS LISS III image and DEM in a rugged terrain: a case study in Himalayas. Geocarto Int 20(2):33–40
Sekertekin A, Marangoz AM, Akcin H (2017) Pixel based classification analysis of land use land cover using sentinel-2 and landsat-8 data. Int Arch Photogramm Remote Sensing Spatial Inf Sci:91–93
Shalaby A, Tateishi R (2007) Remote sensing and GIS for mapping and monitoring land cover and landuse changes in the Northwestern coastal zone of Egypt. Appl Geogr 27(1):28–41
Singh RP, Sahoo AK, Bhoi S, Kumar MG, Bhuiyan CS (2001) Ground deformation of Gujarat earthquake of 26 January. J Geol Soc India 58:209–214
Singh RP, Bhoi S, Sahoo AK, Raj U, Ravindran S (2001) Surface manifestations after the Gujarat earthquake. Curr Sci 81:164–166
Singh RP, Bhoi S, Sahoo AK (2001) Significant changes in the ocean parameters after the Gujarat earthquake. Curr Sci 80:1376–1377
Singh R, Simon B, Joshi PC (2001) Estimation of surface latent heat fluxes from IRSP4/MSMR satellite data. Proc Indian Acad Sci 110:231–238
Singh RP, Bhoi S, Sahoo AK (2002) Changes observed on land and ocean after Gujarat earthquake 26 January 2001 using IRS data. Int J Remote Sens 23:3123–3128

Sinha R, Jain V, Tandon SK (2012) River systems and river science in India: major drivers and challenges. Earth system processes and disaster management. Springer, pp 67–90

Sinha R, Jain V, Tandon S (2013) River systems and river science in India: major drivers and challenges. Earth system processes and disaster management, pp 67–90

USDA Soil Conservation Service (1974) USDA-SCS Soil Survey of Travis County, Texas. College Station, Texas. Texas Agricultural Experiment Station, and Washington, D.C.

Tolessa T, Senbeta F, Kidane M (2017) The impact of land use/land cover change on ecosystem services in the central highlands of Ethiopia. Ecosyst Serv 23:47–54

Trivedi A, Pyasi SK, Galkate RV (2019) Impact of climate change using trend analysis of rainfall, RRL AWBM toolkit, synthetic and arbitrary scenarios. Curr J Appl Sci Technol:1–18

Verburg PH, Veldkamp A, de Koning GHJ, Kok K, Bouma J (1999) A spatial explicit allocation procedure for modelling the pattern of land use change based upon actual land use. Ecol Model 116:45–61

Vitousek PM, Mooney HA, Lubchenco J, Melillo JM (1997) Human domination of Earth's ecosystems. Science 277(5325):494–499

Youssef M, Ali BA (2017) Revival of forgotten rivers through recreating the cultural promenade: a case study of the revival of beirut river, lebanon. Sustain Dev Plann 226:725–737

Zende AM, Devkate S, Atal KR (2015) Selection of suitable sites for water harvesting structures in chand watershed using geospatial techniques. In: 20th international conference on hydraulics. IIT Roorkee, pp 1–8